Estuarine hurricane wind can intensify surge-dominated extreme water level in shallow and converging coastal systems

Mithun Deb[1], James J. Benedict[3], Ning Sun[2], Zhaoqing Yang[1,4], Robert D. Hetland[2], David Judi[2], and Taiping Wang[1]

[1]Marine and Coastal Research Laboratory, Energy and Environment Directorate, Pacific Northwest National Laboratory, Sequim, WA 98382, USA
[2]Energy and Environment Directorate, Pacific Northwest National Laboratory, Richland, WA 99354, USA
[3]Los Alamos National Laboratory, Los Alamos, NM 87544, USA
[4]Department of Civil and Environmental Engineering, University of Washington, Seattle, WA 98195, USA

Correspondence: Mithun Deb (mithun.deb@pnnl.gov)

Abstract. Based on the projected increase in hurricane landfall frequency on the middle to lower U.S. East Coast, we examined the crucial role of the estuarine wind field in exacerbating coastal flooding. A regionally refined atmospheric and two high-resolution hydrology and ocean models are integrated to provide plausible and physically-consistent ensembles of hurricane events and the associated flooding inside the Delaware Bay and River, a U.S. mid-Atlantic estuary. Model results show that 5 the hurricane propagation direction, estuarine geometry, remote surge from the open ocean, and direct nearshore upwind stress could magnify the flood magnitude. More specifically, inland-bound tracks that make landfall before reaching the mid-Atlantic coast produce a more significant surge within Delaware Bay than the shore-parallel tracks, where the estuarine wind direction plays the primary role in surge amplification. Ultimately, this study emphasized the need for integrated models to capture the nonlinear dynamics and interactions in flood hazard modeling.

10 **Plain Language Summary**

This study examines how estuarine wind field can exacerbate hurricane-driven coastal and riverine flooding. We coupled earth system, hydrology, and hydrodynamic models to generate plausible and physically consistent ensembles of hurricane events and their associated water levels from the open coast to tidal rivers of Delaware Bay and River. Our results show that the hurricane landfall locations and the estuarine wind can significantly amplify the extreme surge in a shallow and converging 15 system, especially when the wind direction aligns with the surge propagation direction. Other essential factors, such as the amplitude of the remote surge from the open ocean and the magnitude and timing of peak river discharge, can further amplify the extreme water level. Ultimately, this work demonstrated the need for integrated modeling to capture the wind, tide, and surge interactions during a hurricane landfall and why such a framework is critical for improving coastal hazard projections in a warmer climate.

1 Introduction

Due to their low-lying topography and high population densities, coastal cities and estuaries are particularly susceptible to storm surges, which result in significant economic and social impacts like damage to infrastructure, loss of property and livelihoods, and loss of life (Dietrich et al., 2010; Bilskie et al., 2016; Valle-Levinson et al., 2020). Recent climate studies have indicated that, under different greenhouse gas emission rates and global warming scenarios, there is a potential for more frequent hurricane landfalls on the U.S. Atlantic coast at the end of the 21st century (Knutson et al., 2022; Balaguru et al., 2023). Some other works have shown a potential increase in hurricane's maximum intensity (Emanuel, 2005, 2021), an increase in the 10 m wind speed (Roberts et al., 2020), and a decrease in translation speed (Emanuel, 2021; Garner et al., 2021) in the future. These projected trends in hurricane characteristics can amplify the risk faced by coastal cities and estuaries to storm surges and coastal flooding in the future climate. More recently, using Coupled Model Intercomparison Project Version 5 (CMIP5) global climate model datasets, Weaver and Garner (2023) examined the hurricane landfall patterns in the U.S. East Coast for a warmer climate. They showed a positive trend in hurricane genesis points moving northward and making more landfalls along the mid-Atlantic region as they traveled through the U.S. Northeast (similar to Hurricane Irene 2011). This is a matter of concern for the U.S. mid-Atlantic region that covers two of the largest estuaries in the U.S.: the Delaware and Chesapeake Bays. These estuarine regions house ~ 27 million inhabitants, a large density of metropolitan areas, natural ecosystems (e.g., salt marshes and freshwater wetlands), transportation networks, and industrial ports (Callahan and Leathers, 2021). The hurricane landfall trend in this area certainly raises interest in the associated storm surge hazard that might help develop flood risk assessment tools for federal, state, and local agencies.

To estimate the hurricane-induced flood risk, significant effort has been invested in storm surge prediction using high-resolution numerical models that resolve fundamental underlying physics (Weisberg and Zheng, 2006; Wang et al., 2008; Hu et al., 2009; Dietrich et al., 2011). However, a significant impediment to accurate storm surge predictions continues to be the uncertainty in predicting hurricane properties that drive storm surge (Cyriac et al., 2018; Cangialosi et al., 2020). More specifically, an inaccurate representation of any of these hurricane characteristics: intensity, size, translation speed, and the angle of landfall with the coast can introduce large biases in predicting the surge and coastal flooding. In addition, storm surge also strongly depends on the local geometry of the basin and bathymetric features (e.g., the angle of a coastline), such that an adequate representation of the system's geometry is essential for properly estimating the hydrodynamic response (Resio and Westerink, 2008; Weisberg and Zheng, 2006). Geometry is especially important in estuarine regions, where the storm surge and storm tide (sum of surge and the astronomical tide) propagation and flood generation can vary spatially based on the size and bathymetry of the bay, cross-sectional area, the shape of the system (e.g., funnel-shaped estuary, rectangular shaped tidal lagoons, etc.), and river discharge from the hurricane-induced precipitation (Mori et al., 2014; Familkhalili and Talke, 2016). In general, in hyper-tidal estuaries (exhibit large tidal range) or convergent estuaries (channel area convergence dominates bottom friction), the variability of tide-surge interaction can amplify the extreme water level (Lyddon et al., 2018). In addition, the magnitude and duration of the estuarine winds during hurricane landfall can exacerbate the spatial extent and amplitude of surge-driven flooding (Shen et al., 2006a; Weisberg and Zheng, 2008).

In shallow estuaries, the local wind field can create a surface slope between the bay mouth and the upstream end (Weisberg
55 and Zheng, 2006, 2008). This evolution becomes much more complex for a convergent system where the non-linear interaction
between the tide, surge, and local geometry influences the flow acceleration, ultimately amplifying or damping the surge-
induced flooding (Wong and Moses-Hall, 1998). When the remote surge generated by the wind field in the open ocean reaches
the coastal environment, it interacts with the estuarine wind and generates a complex set-up or set-down within the estuary
(Shen et al., 2006b; Defne et al., 2019). There have been many studies on the storm surge hindcast and long-term flood
60 hazard projections for different coastal or estuarine regions [e.g., Villarini et al. (2014); Wahl et al. (2015); Marsooli et al.
(2019); Lin et al. (2019); Bates et al. (2021); Gori et al. (2022)]; however, the effect of estuarine winds on surge amplification
during hurricane landfall is not often separately analyzed. For several U.S. coastal regions, Lin et al. (2010) and Marsooli
and Lin (2018) used higher-resolution hydrodynamic models to assess the sensitivity of coastal flooding to different storm
characteristics, but they also focused primarily on the overall surge evolution during the entire hurricane period and not on the
65 local amplification by the nearshore wind field during landfall.

Similarly, several other studies used the simplified storm surge model: Sea, Lake and Overland Surges from Hurricanes
[SLOSH; Jelesnianski (1992)] to assess basin-scale flooding from individual extreme events (Powell and Houston, 1996; Hous-
ton et al., 1999) or the ensemble of probabilistic hurricane tracks (Taylor and Glahn, 2008). While these studies extensively
discussed the role of landfall location, wind direction, and coastal geometry, the role of estuarine wind in the local amplification
70 of storm surge remained unexplored. Also, it should be noted that in a system with an irregular bottom and rapidly converging
width, it is challenging to assess the role of estuarine wind using simplified models like SLOSH due to the absence of ad-
vective terms in the momentum equations, exclusion of the river flow and the parametric representation of the hurricane wind
field (Glahn et al., 2009). To properly examine the role of estuarine wind and the non-linear interaction in surge amplification
in a complex system, an integrated modeling framework with higher-order physics is required that resolves the atmospheric,
75 hydrologic, and hydrodynamic processes during hurricane landfall.

This study aimed to answer, depending on the estuarine wind field (i.e., landfall location and wind direction), how different
the hydrodynamic responses during flooding when compared between an inland hurricane (making landfall before reaching
Delaware Bay) and a shore-parallel track (making landfall after passing Delaware Bay). This is an important question because
of the potential changes in landfall trends in a warmer climate in the U.S. Mid-Atlantic region. We focused on two tasks:
80 1) integrating an earth system model [E3SM, Golaz et al. (2022)] with high-resolution models that couple the hydrology
[DHSVM, Wigmosta et al. (1994)] and hydrodynamic [FVCOM, Chen et al. (2003)] models to provide a high-fidelity flood
estimate, and 2) evaluating the role of the estuarine wind field in amplifying storm surge during hurricane landfall. We chose
Delaware Bay and River (DBR), a shallow and convergent estuary in the U.S. Mid-Atlantic, historically highly vulnerable
to storm-induced flooding. We also selected Hurricane Irene (2011) as a focal event for the study, which caused one of the
85 most severe estuary-wide flood hazards in DBR. Using E3SM, we first perturbed Hurricane Irene (2011) to get an ensemble
of Irene-like tracks with different characteristics. Then using the coupled DHSVM-FVCOM, we predicted the total water level
from different tracks and the flood distribution along the entire DBR. Incorporating these three models provided a high-fidelity
representation of coupled atmospheric, fluvial, and coastal processes, which allows for improved flood estimates for Hurricane

Irene-like events. Finally, we separately looked at the role of the estuarine wind field in amplifying the surge as the tide

90   propagates upstream.

(a) E3SM model domain

(b) DHSVM and FVCOM model domains

(c) Delaware Bay and River

(d) Integrated model workflow
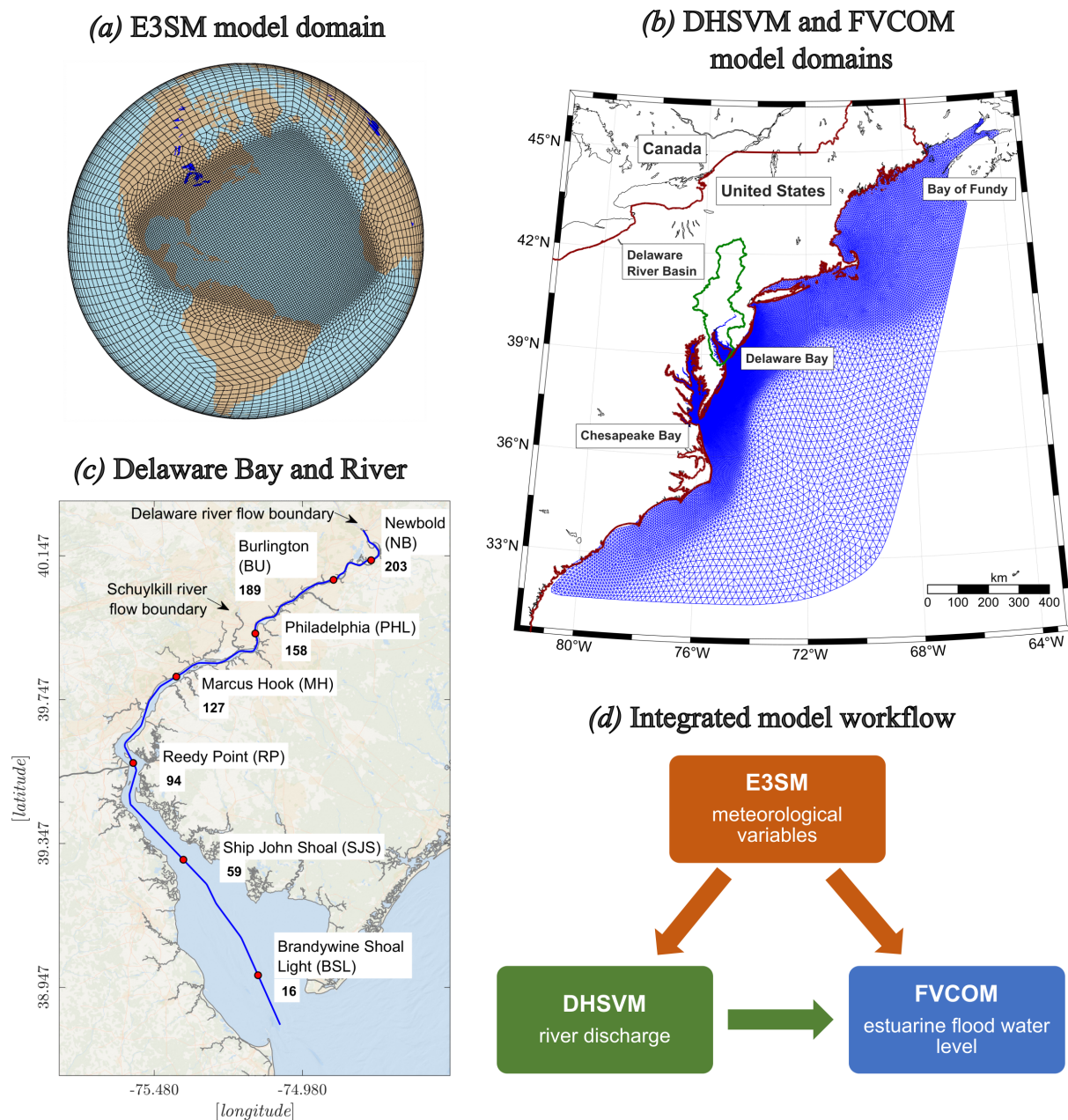
Figure 1. (a) E3SM grid resolution: 100-km globally uniform resolution and a 25-km resolution over the North Atlantic; (b) Regional scale model domains, where blue triangles show the FVCOM grid cells and green polygon represent the DHSVM model coverage; (c) Focus area of the study, Delaware Bay and River (DBR). Red circles show tide gauge locations used for FVCOM model validation with their distance from the Bay mouth (in kilometers); (d) Schematic showing the coupling strategy between the different models used in this study.

2 Model setup and integration

The U.S. DOE Energy Exascale Earth System Model version 2 [hereafter, "E3SM"; Golaz et al. (2022)] is used to simulate an ensemble of Hurricane Irene-like tracks. E3SM integrations are conducted using prognostic atmosphere, land, and river model components, while oceanic sea-surface temperatures (SSTs) and sea ice cover are prescribed based on observations

95 (Huang et al., 2021). The atmosphere model has 71 levels and uses a regionally refined horizontal grid mesh of ∼25 km over the North Atlantic basin and eastern North America with a coarser horizontal resolution (∼100 km) outside this region (Fig. 1a). The atmosphere model is initialized globally based on ECMWF Reanalysis version 5 [ERA5; Hersbach et al. (2020)], and all simulations span 30 days to cover the atmospheric spin-up and evolution of Hurricane Irene as well as the meteorological conditions in the wake of the event. Additional details of the E3SM setup and validation metrics are found in Appendix A.

100 We conduct an E3SM ensemble to acknowledge (a) our incomplete understanding of the model physics and (b) the inherent uncertainty of model initial conditions. To address (a), we perturb model physics parameters to which tropical cyclones are most sensitive [He and Posselt (2015); see Appendix A for the list of perturbed parameters]. This is accomplished by first defining acceptable numerical ranges for each parameter of interest and then randomly drawing 50 values within those ranges to use within the model integration. In this way, 50 unique parameter "sets" are created. To address (b), E3SM is initialized at

105 two times separated by 12 hours [26 August 2011 00Z (hereafter "E1") and 25 August 2011 12:00Z (hereafter "E2")]. E1 was identified as the optimal initialization time that produced reasonable Irene tracks at the earliest forecast lead time, while E2 was also retained to understand the sensitivities of the predicted tracks to large-scale meteorological patterns at initialization time. In total, two 50-member ensembles (E1 and E2) are generated (Figure 2a).

Subsequently, we employ the Distributed Hydrology Soil Vegetation Model (DHSVM) to estimate the fluvial flooding in

110 the Delaware River Basin. DHSVM used meteorological variables from the E3SM model as climate forcing, including precipitation, air temperature, downward shortwave and longwave radiation, wind speed, and relative humidity. DHSVM is a process-based, spatially distributed hydrological model that operates at the grid cell level. It simulates key overland and subsurface hydrological processes by solving the full energy and water balance equations. The model physics and formulations have been extensively described in the existing literature [e.g., Wigmosta et al. (1994); Sun et al. (2015); Perkins et al. (2019)].

115 For this study, we used a 90-m resolution for DHSVM in the Delaware River Basin and ran the model at a 3-hourly timestep.

Finally, to predict the extreme water surface elevation (WSE) with the atmospheric and riverine forcings, we use the unstructured grid Finite Volume Community Ocean Model FVCOM (Chen et al., 2003), which has been extensively used for storm surge modeling in many estuaries worldwide [e.g., Weisberg and Zheng (2006); Rego and Li (2009)]. We chose the 3D barotropic and hydrostatic version, which resolves simplified Reynolds-averaged Navier–Stokes equations (with Boussinesq

120 approximations). The model domain extends 700 km offshore from the mid-Atlantic coast to adequately capture the air-sea interaction and 215 km from the Delaware Bay mouth to the river flow boundary (Figure 1b,c). The horizontal grid resolution is assigned to 25 km along the open ocean boundary to 20 m in the river to seamlessly simulate the interaction between large- and small-scale flood processes. Subsequently, we enforced the lateral and sea surface boundary conditions: 1) tidal forcing at the open ocean boundary [WSE from the TPXO8.0 global ocean tide model (Egbert and Erofeeva, 2002)], 2) river flow from

125 DHSVM, and 3) 10-m wind speed and mean sea-level pressure from E3SM. More details about the topography and bathymetry data sets used for grid development, activated model physics, and assigned numerical variables/coefficients are given in Deb et al. (2023).

3   Hurricane-induced estuarine flooding

At the onset, DHSVM simulated daily flows (averaged from the 3-hourly flows) were validated against USGS daily flow
130   observations at six gage locations on the main stem of the Delaware River for Hurricane Irene (2011) [Appendix B]. After observing a satisfactory model performance (Nash-Sutcliffe efficiency and the Kling–Gupta efficiency), we simulated the E3SM ensembles that produced a different range of peak river discharge at the Delaware River boundary, shown in Figure 2b. The range and the ensemble mean of the river discharge from the two sets show a clear distinction, where the inland-oriented tracks (E2) produced a smaller magnitude and an earlier peak ($\sim 12\,hours$) compared to the shore-parallel tracks (E1). In
135   this work, as we focused on the response of estuarine flooding to different hurricane characteristics, we directly used the DHSVM data as river forcing for FVCOM without discussing the underlying physical processes responsible for the variation in magnitude and phase of the fluvial discharge.

Before running FVCOM with meteorological conditions from E3SM and river forcing from DHSVM, we also validated the hydrodynamic model by comparing predicted WSE with the observed data for two hurricanes, Hurricane Irene (2011)
140   and Hurricane Sandy (2012), that both had devastating impact on DBR. For both cases, we found that the model successfully predicts the amplitude and phase of the storm surge and shows an excellent agreement between the model and observed data at various tide gauge locations throughout the system [Appendix C]. Thus, the model was deemed fit for purpose for our subsequent studies using ensemble forcing.

The ensemble simulations, forced with two 50-member ensembles of Irene-like cases (E1 and E2), show significant variabil-
145   ity ($\mathcal{O}(1\,m)$ standard deviation in WSE) in the range of along-channel peak WSE over the ensemble forcing (Figure 2c). E2, with more inland tracks, generates a much higher range of surge than E1 for a significant portion of DBR; E2 also has a significantly higher ensemble mean WSE, especially in the mid-bay approximately 150 km from the mouth, where the E2-forced ensemble mean WSE is over 2 m higher ($\sim 100\%$ increase) than the E1-forced case.

Interestingly, close to the bay mouth and near the upstream river boundary, the distribution of E1- and E2-forced WSE
150   are similar, despite strong differences in the mid-bay. The similarity at the bay mouth indicates that the offshore hurricane wind field (outside the bay) generated a narrow range of the remote surge, which propagated upstream from the bay entrance. Then, there is a local generation of storm surge inside the bay (between BSL and BU), significantly higher for E2, likely due to a combination of the hurricane's estuarine wind field and convergence of the estuarine width. The river discharge plays a secondary role; we can see that for E1, which produces a much higher flux magnitude, the impact is only significant for the
155   region between BU and NB (the narrowest portion near the DHSVM flow boundary). In general, for all the tracks from E1 and E2, the peak river discharge at the Delaware River boundary lagged the storm surge at the bay entrance by two days, making the impact of river discharge negligible during the landfall period on Aug/28/2011 12:00Z. The higher surface slope

near the river boundary for E1, shown in Figure 2c, was generated primarily from the peak river discharge that occurred around Aug/30/2011 12:00Z (Figure 2b). While a similar along-channel gradient can also generate for E2 around Aug/30/2011 12:00Z,

160 the significantly higher surge during the landfall (Aug/28/2011 12:00Z) elevated the peak WSE much more than the following river discharge-driven condition. A more detailed explanation of this WSE variation is given in the following section.
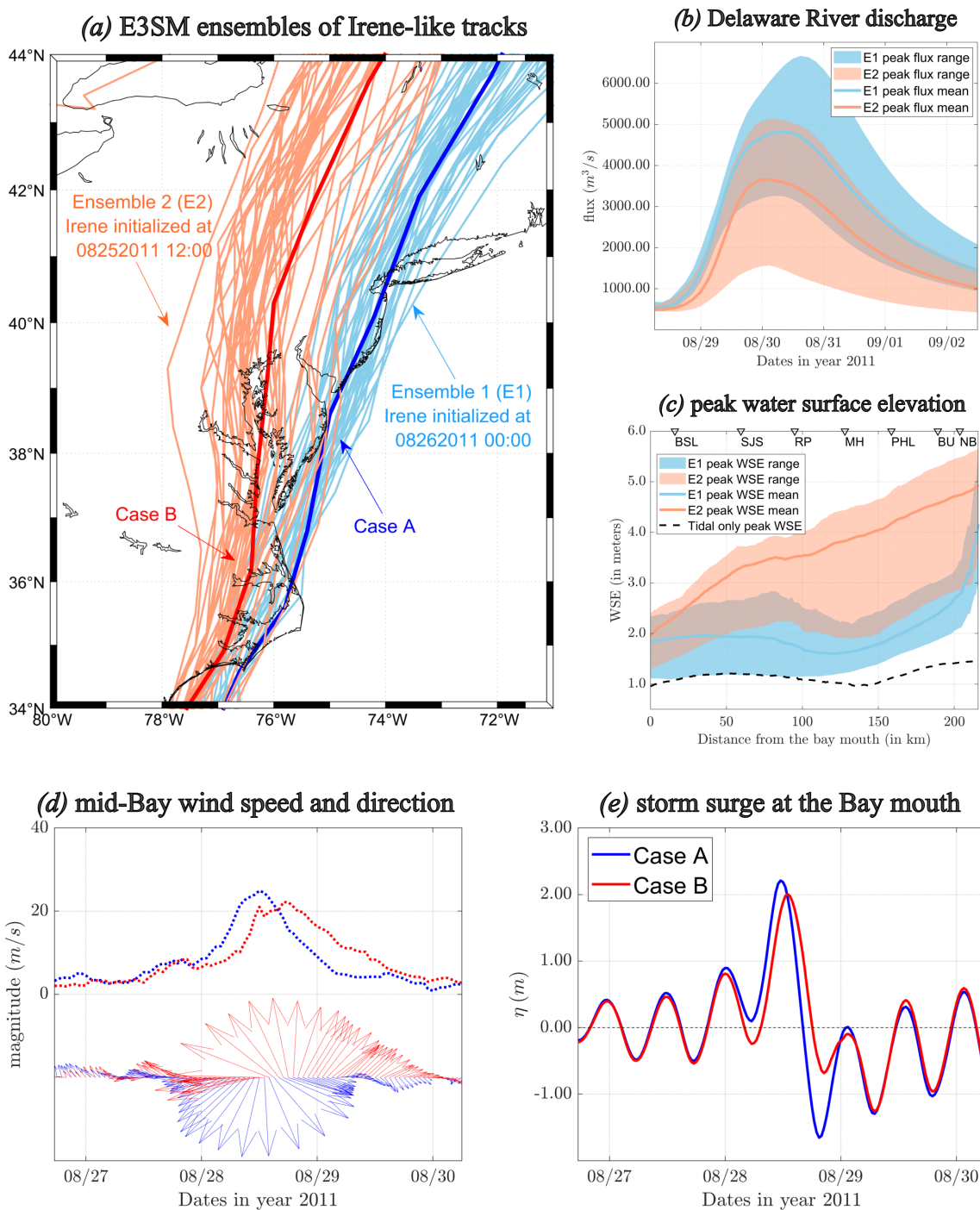
Figure 2. (a) Ensembles of hurricane Irene-like tracks generated using E3SM; (b) Delaware River discharge for the tracks in (a) by DHSVM; (c) Predicted peak water surface in DBR using FVCOM; (d) Estuarine wind speed and direction for Cases A and B; (e) Storm surge elevation for the same events.

4 The role of local estuarine wind in surge amplification

In this section, we examined the impact of estuarine wind directions in amplifying storm surges along the converging DBR system. We selected two tracks from the ensembles – Cases A from E1, and B from E2 (Figure 2a) – that produced a nearly

165 similar surge at the Delaware Bay mouth (the 'remote surge' hereafter), shown in Figure 2e. Cases A and B also have comparable 10-m elevation wind magnitudes inside the bay (Figure 2d), though the strongest winds are in opposite directions; Case A with a primarily northerly wind, and Case B a southerly wind.

Figures 3a,b shows a 2D representation of hurricane wind field for the two events when the estuarine wind speed peaked ($\sim 20\,m/s$) inside DBR. To isolate the role of estuarine wind, we defined a region (the black polygon in Figures 3a,b) that

170 covers the hydrodynamic model domain from the bay mouth to the upstream model boundary. Figures 3c and 3d show the instantaneous WSE along the main channel for the two tracks based on simulations with and without the effect of estuarine wind fields within the defined region.

It is evident that the local estuarine wind stress plays a significant role in both cases in altering WSE as the storm surge propagates upstream. However, the estuarine wind plays a more prominent role in Case B, where the southerly wind is directed

175 up-channel, and pushes more water northward into the converging portion of the Bay, resulting in a rapid increase in the water level from BSL to NB (Figure 2c). In contrast, Case A shows a markedly different response within the system, as the northerly wind causes a set-down at the upstream portion of DBR and a set-up in the mid-bay resulting from the interaction of the local and remote surge, which produced higher flooding ($\sim 1.0\,m$) between SJS and PHL (Figure 3c).

Previous studies have demonstrated how the local estuarine wind field created surface slope during hurricane landfalls at

180 Tampa Bay, FL (Weisberg and Zheng, 2006), and Chesapeake Bay, VA (Shen et al., 2006b), respectively. They have shown that, in shallow estuaries, the cross-shore component of wind stress creates a large downwind surface slope and surge. To explain this process mechanistically, Wong and Trowbridge (1990) and Shen et al. (2006a) provided linear solutions for WSE along a hypothetical rectangular estuary by dividing the total water level into two parts: remote surge and set-up/set-down from local wind forcing. While the linear and simplified momentum equations (using a constant bottom and width of the

185 estuary) can provide a fundamental understanding of the spatially-varying surge amplitude, the evolution of flooding becomes much more complex for a convergent system. In such cases, the non-linear interaction between the tide, surge, and local geometry may increase or decrease along-channel WSE (Weisberg and Zheng, 2008; Xiao et al., 2021). In a complex system with irregular bottom and rapidly converging estuary width like DBR, the simplified equations cannot reasonably predict the surface variation shown in Figures 3c,d, and a high-resolution 3D numerical modeling framework is necessary to address the

190 non-linear interactions and the associated surge generation.

The evolution of peak WSE for the entire period of the hurricanes was examined by designing a few scenarios to identify the primary drivers of estuarine storm surge intensity. In the hydrodynamic model run, surface wind stresses (estuarine, remote, and both) were included along with the tidal forcing in a sequence to explain the incremental flood amplification, shown in Figures 4a,b. For Case A (with a northerly wind from E1), the estuarine wind aligned against the incident tidal wave (without remote

195 surge) and produced a steep slope between MH and SJS due to the complex tide-wind interaction and channel convergence. The

downwind water surface pressure gradient in the estuary caused additional resistance to the propagating flood tide. Combined with the convergence effect, this non-linear interaction amplified the bay water level (Figure 4a). When the full wind field is included, we can see a similar along-channel peak WSE gradient where the only difference in water level ($\sim 1.0\,m$) came from the remote surge propagation through Delaware Bay. Figure 4a also shows that the remote surge, as it travels through the system, follows a similar trend of the peak tidal WSE where some amplitude damping occurs close to RP due to higher flooding of the surrounding low-lying wetlands. The combined effect of the remote surge and local set-up from the estuarine wind field attributed to a locally amplified flooding on the bay-river interaction zone (between SJS and MH), where the peak water surface increased by more than $1.0\,m$ ($\sim 60\%$) at certain locations. A spatial map of the peak WSE difference between surge from the full wind field and the remote field only ($\Delta\eta$ in meters) is given in Figure 4c to demonstrate the extent of the flooding in the same zone. Finally, when the river discharge from the hurricane precipitation field is added to the full wind simulation, it seems to generate a steep WSE gradient and compound flooding on the upstream part of the Delaware River (Figure 4a), where the river width is significantly narrower than the estuary and bay mouth.

Case B, with a southerly wind, shows much higher flooding (almost doubled near the head) for the full simulation than Case A (Figure 4b). As the estuarine wind and remote surge propagated in the same direction, the direct upwind push of the water from the large bay surface raised the peak WSE from BSL to the upstream model boundary. While we can see a change in the water surface slope near SJS from the higher overland flooding, the combined WSE from wind-generated local surge and remote surge demonstrate a linear increase along the channel. Between BSL and SJS, the estuarine wind and remote surge interacted similarly to the previous observations of Wong and Trowbridge (1990) and Shen et al. (2006a). However, from SJS to the remaining narrow reach, the channel cross-section area convergence amplified the peak WSE as the wave propagated upstream. Compared to the remote surge-only case, the combined estuarine wind and remote surge case produced a 2 m higher water surface elevation ($\sim 100\%$ increase). The inclusion of river discharge did not make any notable difference in the upstream regions (as seen in Case A) due to the larger surge-driven channel water volume and surface area. Figure 4d shows the peak WSE difference ($\Delta\eta$) for Case B, where we see a dramatic increase in along-channel flooding from the estuarine wind field. This case illustrates that the local estuarine wind stress can significantly amplify WSE from the bay entrance to upstream regions in converging estuaries (nearly $2.5\,m$ or 150% for Case B), even when the offshore surge near the entrance is not catastrophic.
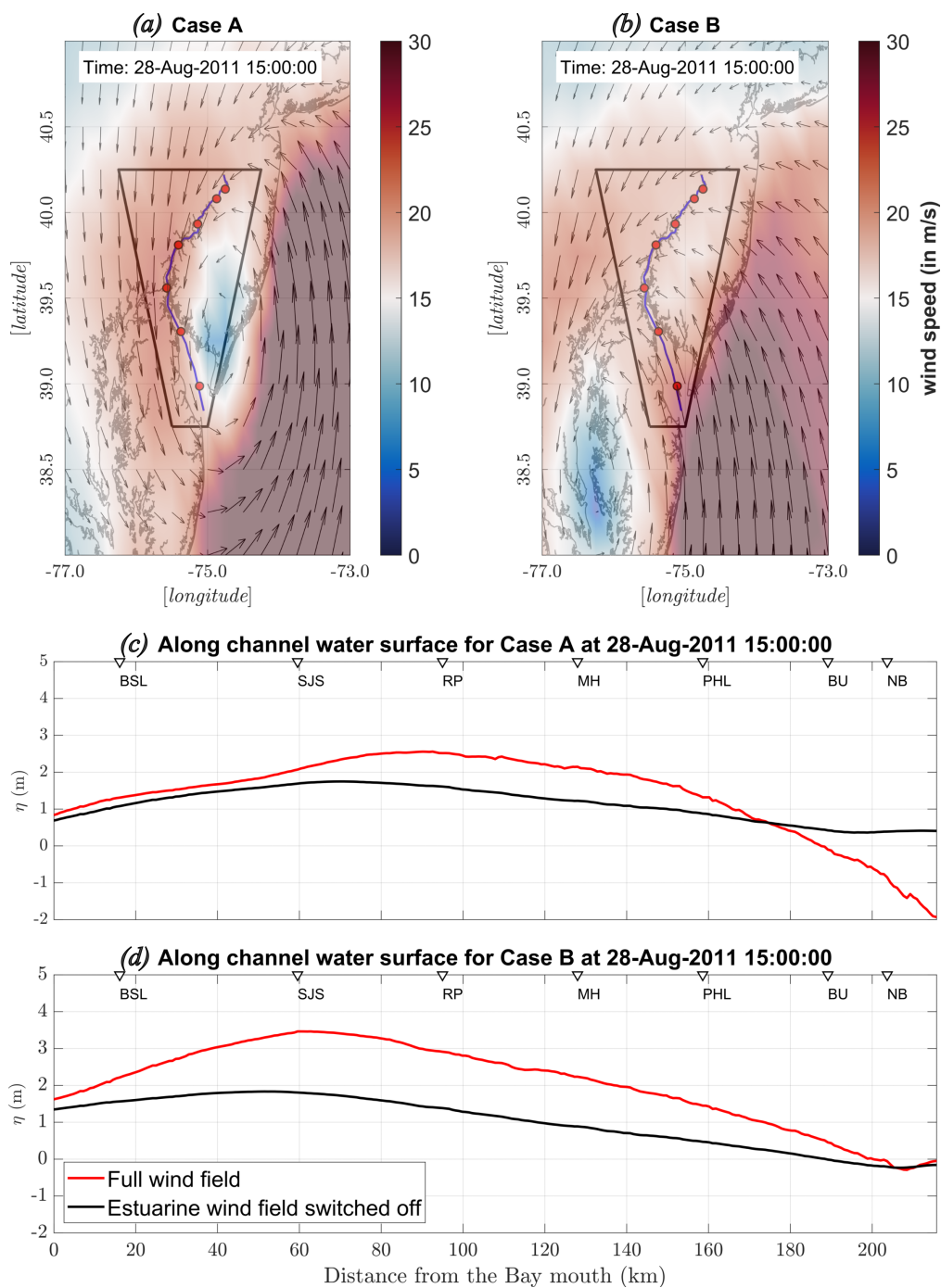
Figure 3. (a,b) Instantaneous 10-m elevation wind field during the landfall for hurricane Cases A and B. Polygon shape drawn on top of DBR to represent the region used to dampen the wind stress; (c,d) Comparison of the instantaneous along-channel water surface with and without the estuarine wind for both cases.
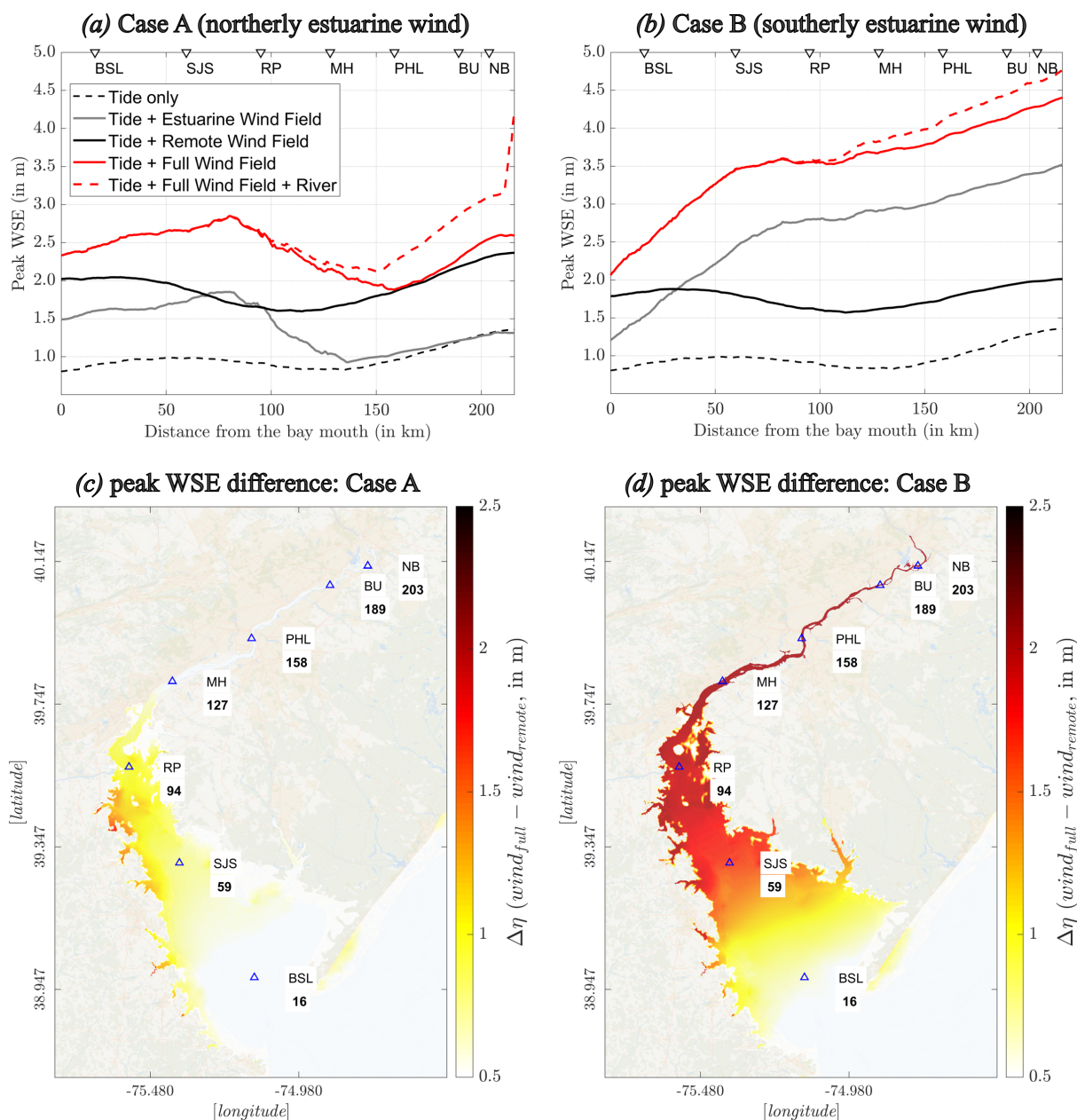
Figure 4. (a,b) Changes to along-channel peak water surface elevation for different force combinations for Cases A and B; (c,d) The difference in peak water surface with and without estuarine wind for the same cases.

5   Discussion and conclusions

This study examined the role of different hurricane landfall locations and the associated estuarine wind field on the local amplification of storm surges in a converging coastal system. A key finding was that small differences in hurricane tracks

225   could cause drastic differences in the bay surface wind stress (time scale is on the order of hours) and the along-channel storm surge response due to local geometry. Previous works related to the sensitivity of storm surge and coastal flooding to hurricane landfall locations, wind field (speed and direction), and geometry have not separately examined the role of this shorter period (translation period through the estuary) and estuarine-scale landfalling wind using physics-based integrated modeling frameworks.

230   Thus, there is a clear need to better understand the complex, nonlinear response of storm surge to storm track, as simple metrics such as distance to storm track could be misleading and fail to capture the intricacies of the response. Further work is also needed to examine the role of hurricane intensity, the radius of maximum wind, and translation speed separately, all of which could influence local surge response as the hurricane track. These essential hurricane characteristics can affect both the remote and local surge generation, requiring a future study focusing on their overall impact on the same area. Also, this work

235   emphasized the utility of a model hierarchy, which is crucial for accurately representing important localized factors such as the estuarine wind field. This approach is essential for improving future coastal hazard projections on the U.S. Atlantic coast for a warmer climate.

The integrated modeling framework combining an earth system model (E3SM), hydrology model (DHSVM), and hydro-dynamic model (FVCOM) helped generate plausible and physically-consistent two ensembles of hurricane Irene-like events,

240   associated river discharge, and the coastal flood water level, respectively. Peak water surface elevation inside Delaware Bay and River, a shallow and convergent system, showed a pivotal relationship with the estuarine wind directions. Even though tracks in Ensemble 2 (inland hurricanes) made landfall much earlier before reaching the bay compared to Ensemble 1 (shore-parallel hurricanes), and both had a similar storm surge magnitude at the bay mouth (propagated from the open ocean), the inland-oriented tracks produced greater flooding inside the bay and river despite much smaller river discharge. Upon examining the

245   flood generation mechanisms step-by-step, we observed that the estuarine hurricane wind could significantly amplify flooding in shallow and converging estuaries when it follows the surge propagation direction. Case B, which has shown this effect, produced nearly $2.5\,m$ or 150% increase in the peak WSE from the bay entrance to the upstream river portion compared to the case with remote surge only. The water surface gradient demonstrated a spatially-varying effect of the non-linear interaction between tide, surge, wind stress, and the estuary geometry, where the channel convergence rapidly raised the peak WSE as the

250   flood wave propagated upstream. When the surge and estuarine wind direction opposed each other (as seen for Ensemble 1), the complex interaction produced a set-down in the river, a set-up in the bay, and a higher surge in the middle of the estuary. As shown for Case A, while the flooding is limited to the mid-portion of the estuary, the peak WSE increased again by more than 60% compared to the case without bay surface wind stress.

Ultimately, the analysis showed that even if a hurricane makes landfall before reaching the mid-Atlantic region and does not

255   bring a record extreme water level near the bay mouth from offshore, the direct upwind forcing over the estuarine surface area

itself can produce a record level of flooding if it aligns with the surge direction. In converging estuarine systems worldwide [e.g., the Delaware Bay and River (USA), the Meghna River Estuary (Bangladesh), and the Pearl River Estuary (China)] that are extremely vulnerable to hurricane-induced flooding, physically consistent and integrated modeling frameworks will be critical to properly resolve this nonlinear tide-wind-surge dynamics and improve the coastal hazard projections for a future

260   climate.

Code and data availability. ECMWF Reanalysis version 5 data were obtained from https://doi.org/10.24381/cds.bd0915c6. NOAA OI-SST version 2 data were obtained from: https://www.psl.noaa.gov/data/gridded/data.noaa.oisst.v2.highres.html. The E3SM version 2 code base is accessible via a Github repository at https://github.com/E3SM-Project/E3SM. The 3D ocean model FVCOM code is available from the MEDM Lab (https://github.com/FVCOM-GitHub). The Distributed Hydrology Soil Vegetation Model (DHSVM) code is available at

265   https://www.pnnl.gov/projects/distributed-hydrology-soil-vegetation-model. Hydrodynamic model tidal boundary conditions are assigned using OSU TPXO Tide Models (https://www.tpxo.net/home), and model validations are performed using tidal water level from NOAA tides and currents (https://tidesandcurrents.noaa.gov/). Model data sets used for further analysis are provided here at https://doi.org/10.5281/zenodo.7988098.

Appendix A: E3SM setup and validation

270 The U.S. DOE Energy Exascale Earth System Model version 2 [hereafter, "E3SM"; Golaz et al. (2022)] land model shares the same horizontal grid as the atmosphere model (described in the main text). The E3SM river runoff model uses a horizontal grid mesh of ∼12 km, though output from this component is not addressed in this study. The atmosphere model is initialized globally using ECMWF Reanalysis version 5 [ERA5; Hersbach et al. (2020)], while initial conditions for the land and river models are taken from the end of a 1 yr E3SM simulation forced by observed, time-evolving atmospheric data. In total, two

275 50-member ensembles are generated by initializing E3SM at two times separated by 12 hours [26 August 2011 00Z (hereafter "E1") and 25 August 2011 12:00Z (hereafter "E2")]. Each ensemble member within E1 uses a unique parameter set, with the same parameter sets being imposed on E2 members (i.e., E2 member N uses the same parameter values as E1 member N, despite different initialization times). The listing of perturbed parameters and their selected ranges appear in Table A1.

Table A1: List of E3SM atmospheric physics parameters modified in this study, including the associated parameterization scheme; default values and minimum and maximum ranges used, and a short description. Parameter value ranges are taken from He and Posselt (2015). For a description of parameterization schemes, see Golaz et al. (2022).

Scheme	Parameter	Default	Min	Max	Short Description
CLUBB	$clubb\_c\_k10$	0.35	0.2	0.6	Coefficient of momentum diffusivity, Kh_zm
ZM	$zmconv\_c0\_ocn$	0.002	0.001	0.0045	Autoconversion coefficient over ocean for deep convection
	$zmconv\_dmpdz$	$-0.7e^{-3}$	-0.002	0.	Parcel fractional mass entrainment rate
	$zmconv\_tau$	3600.	1800.	28800.	Time scale for consumption rate of CAPE for deep convection
MG2	ice_sed_ai	500	50	1400	Cloud ice fall speed parameter

The E3SM Hurricane Irene simulations are evaluated using the National Centers for Environmental Information (NCEI)

280 International Best Track Archive for Climate Stewardship (IBTrACS; Knapp et al., 2010, 2018) to assess hurricane characteristics. Figure A1 displays the time evolution of errors in along- and cross-track distances, minimum central sea-level pressure, and maximum surface wind associated with Hurricane Irene simulated by E3SM initialized at 00Z on August 26, 2011 (ensemble E1). Similar time series for ensemble E2 (not shown) indicate larger distance errors—consistent with a more westward/inland track—but similar errors in minimum central pressure and maximum surface winds, by construction. Figure

285 A1 shows that Hurricane Irene simulated for E1 generally follows the correct trajectory (cross-track errors less than 20 km) but

has a forward speed that is slower than observed (along-track errors of roughly −50 to −100 km). Further, the E1 version of Irene predicts a central pressure that is too low and surface winds that are too high, indicating an overestimation of hurricane intensity.
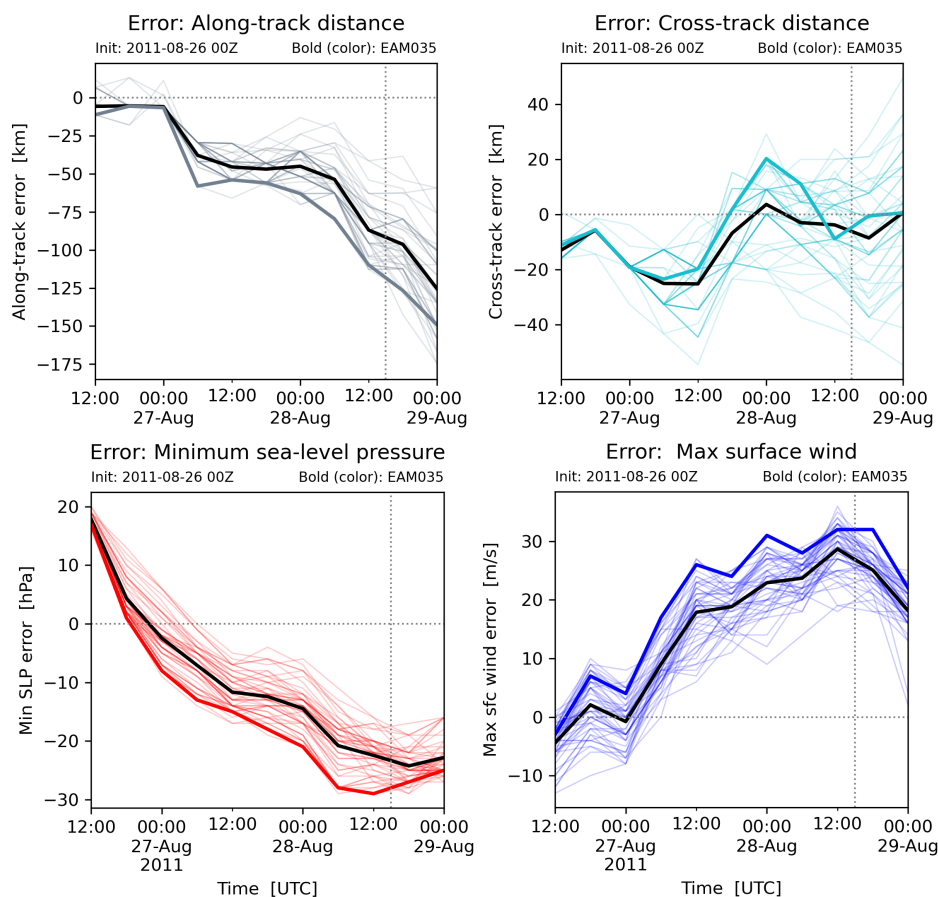
Figure A1. (Upper left) Time-evolving, along-track distance error (simulation minus observations) for E3SM ensemble members (light gray), the ensemble mean (bold black), and the selected ensemble member analyzed in this study (bold gray) for the Hurricane Irene initialized at 00:00Z on August 26, 2011. (Upper right, lower left, lower right) As in the upper left panel, but for the cross-track error, minimum sea-level pressure error, and maximum surface wind, respectively. The gray dotted line marks 15Z August 28, 2011, the time corresponding to the snapshot of Hurricane Irene shown in Fig. 2.

We also use the Climate Prediction Center "Unified Gauge-Based Analysis of Daily Precipitation over CONUS" product
290 (Chen et al., 2008), provided at daily resolution on a 0.25°×0.25° horizontal grid, to assess space-time averaged precipitation accumulations. Figure A2 displays the evolution of mid-Atlantic watershed-averaged (left) 3-hourly precipitation amounts and (right) cumulative sum of precipitation. Watershed-averaged precipitation intensity peaks near 15Z-18Z August 28, 2011 for both the ensemble mean and selected E1 member. E3SM exhibits a slow onset of the watershed-averaged cumulative sum

of precipitation through 12Z August 28, 2011 (Fig. A2, right), but later overestimates cumulative precipitation through 12Z
295 August 29, 2011. This equates to a ~15 mm (~20%) underestimation of cumulative precipitation during the initial impact
window but a ~30 mm (~33%) overestimation of storm-total precipitation. Together, Figs. A1 and A2 indicate that E3SM
simulates a version of Irene that is too slow and too strong, leading to a delayed onset of precipitation in the mid-Atlantic
watershed but ultimately an overestimation of storm-total precipitation.
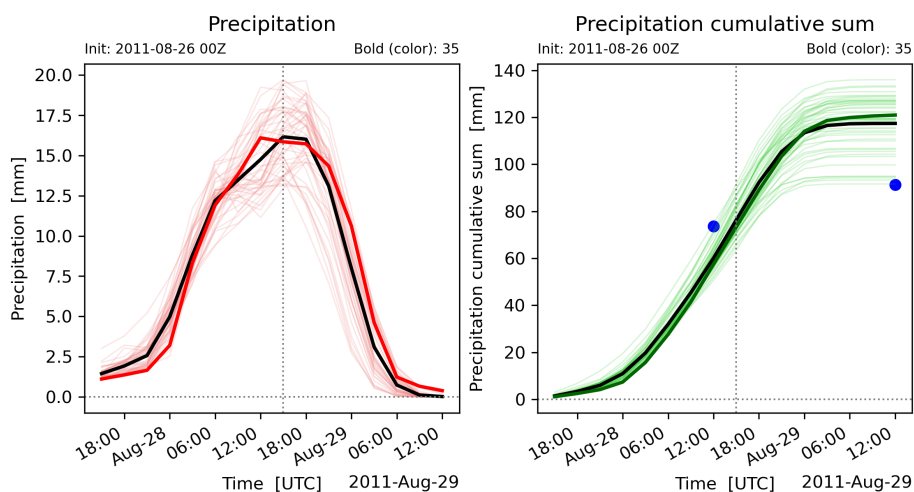
Figure A2. (Left) Time evolution of 3-hourly precipitation amount averaged across the mid-Atlantic HUC2 watershed for E3SM ensemble
members (light red), the ensemble mean (black), and the selected ensemble member analyzed in this study (bold red) for the Hurricane Irene
initialized at 00:00Z on August 26, 2011. (Right) As in the left panel, but for the cumulative sum of watershed-averaged precipitation from
12Z August 27, 2011 through 12Z August 29, 2011, representing the time window of Irene precipitation impacts on the watershed. In the
right panel, CPC rain gauge values are shown as blue dots and indicate cumulative sums for the 24-hour period ending at the time plotted.

Appendix B: DHSVM validation

To evaluate the hydrological model for its robustness in capturing the spatial and temporal variability of flow responses, we chose Hurricane Irene (2011) as the focal event and used a gridded ($\sim 6\,km$) CONUS-scale meteorological dataset developed by Livneh et al. (2013) for model forcing. The source Livneh dataset consists of daily records of precipitation, maximum and minimum air temperature, and wind speed over the period 1950–2013, and they were disaggregated from the daily records to the 3-hourly interval. Then, we evaluated the DHSVM simulated daily flows (averaged from the 3-hourly flows) against the United States Geological Survey (USGS) daily flow observations at six gage locations. These locations represented a range of drainage areas from 4118 - 17560 sq. km along the longitudinal profile (upstream–downstream) of the main stem of the Delaware River (Figure B1a). The model performance was measured using Nash-Sutcliffe efficiency (NSE) and the Kling–Gupta efficiency [KGE; Gupta et al. (2009)]; they are commonly used for measuring hydrological model performance and can be estimated as

$$NSE = 1 - \frac{\sum_{n=1}^{N}(O_n - M_n)^2}{\sum_{n=1}^{N}(O_n - \bar{O})^2} \tag{B1}$$

Where M_n and O_n are simulated and observed daily flow, respectively, N is the total number of days used in metric calculations, and $\overline{O}$ is observed daily mean flow over N days.

$$KGE = 1 - \sqrt{(r-1)^2 + (\alpha-1)^2 + (\beta-1)^2} \tag{B2}$$

Where r is the linear correlation, α is the viability error, and β is the bias between observed and simulated daily flows. Both NSE and KGE range from $-\infty$ to 1, and a value of 1 indicates perfect agreement between simulation and observations.

The comparison between simulations and observations of daily streamflow is shown in Figure B1b. We observed a good agreement for Hurricane Irene (2011), where NSE daily range is from 0.71 - 0.91, and KGE range is from 0.59 - 0.91. Even though the model captured the timing of peak river discharge for all evaluated gages, a higher peak flow bias is observed at USGS-01428500 and USGS-01463500. Among various factors that might have attributed to this bias, some key sources are uncertainties in climate input and topography and the uncertainty in stage-discharge rating curves and streamflow records.
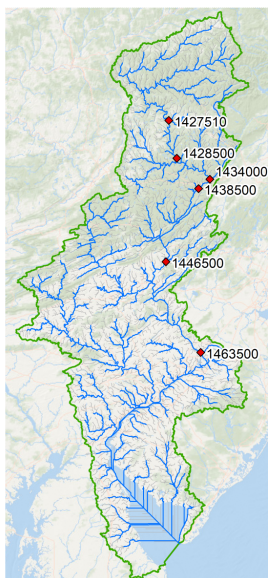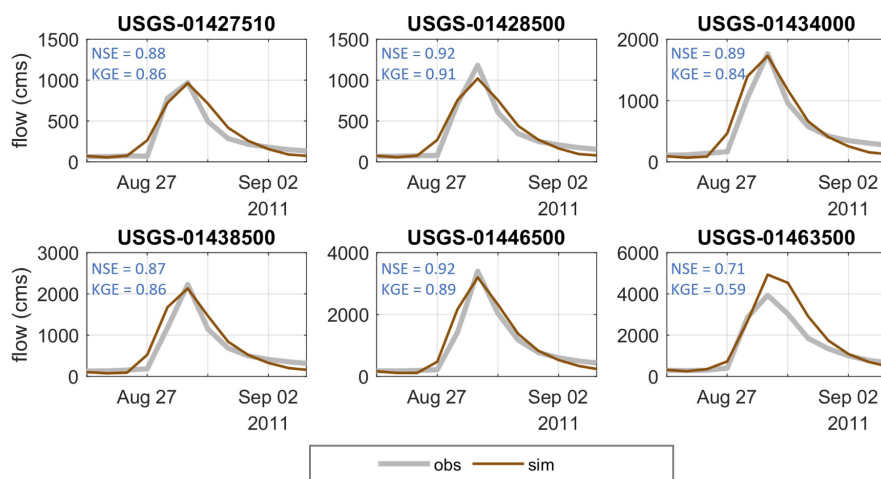
Figure B1. (a) USGS stream gage locations in the Delaware River Basin; (b) Comparison between observed and simulated river discharge at the USGS stream gage locations.

Appendix C: FVCOM validation

To validate the FVCOM model results, we used a different set of model forcing than the one mentioned in the main text (section 2). The sea surface wind stress and atmospheric pressure field of Hurricane Irene (2011) were collected from ERA5, a global atmospheric reanalysis model that provided the highest resolution from the available public data – a spatial resolution
325 of 30 km. As the hydrology model (DHSVM) was only calibrated for Hurricane Irene (2011), for validating FVCOM for both Hurricanes Irene (2011) and Sandy (2012), we assigned the river flow condition using USGS stream gages available at the Delaware River and Schuylkill River model boundary. Also, we collected water surface elevation (WSE) data from the NOAA Tides & Currents database (tidesandcurrents.noaa.gov) for model validation. Finally, to quantify FVCOM model WSE error statistics, we estimated the linear correlation coefficient (corr), average bias index (bias), and model skill as

330
$$corr = \frac{\sum_{n=1}^{N} \left(M_n - \bar{M} \right) \left(O_n - \bar{O} \right)}{\sqrt{\left(\sum_{n=1}^{N} \left(O_n - \bar{O} \right)^2 \right) \left(\sum_{n=1}^{N} \left(M_n - \bar{M} \right)^2 \right)}} \tag{C1}$$

$$bias = \frac{\sum_{n=1}^{N} \left(M_n - O_n \right)}{\sum_{n=1}^{N} O_n} \tag{C2}$$

$$skill = 1 - \frac{\sum_{n=1}^{N} \left(M_n - O_n \right)^2}{\sum_{n=1}^{N} \left(\left| M_n - \bar{O} \right| + \left| O_n - \bar{O} \right| \right)^2} \tag{C3}$$

Where M_n and O_n are simulated and observed water surface elevation, respectively, N is the total number of samples used in metric calculations, and $\overline{M}$ and $\overline{O}$ are the mean of the samples.
335   Figure C1 shows that the model WSE and phase match very well with the in situ WSE and show a strong ability to predict the peak surge elevation for both hurricanes. While the model peak surface amplitude agrees well, even in Philadelphia, there is a slightly elevated amplitude error after the landfall period of Hurricane Sandy (2012). This could be from the missing sub-tidal elevation at the model north-western open boundary, where we have a smaller area coverage for the ocean. The error estimates are shown in the scatter plot (Figure C2), where we only included gauges representing different estuary and river-dominant
340 zones. Overall, the correlation coefficient varies from 0.92 to 0.96, and the skill score from 0.92 to 0.98, respectively, and the averaged bias index indicates a model underprediction due to a slightly elevated tidal damping during the flood.
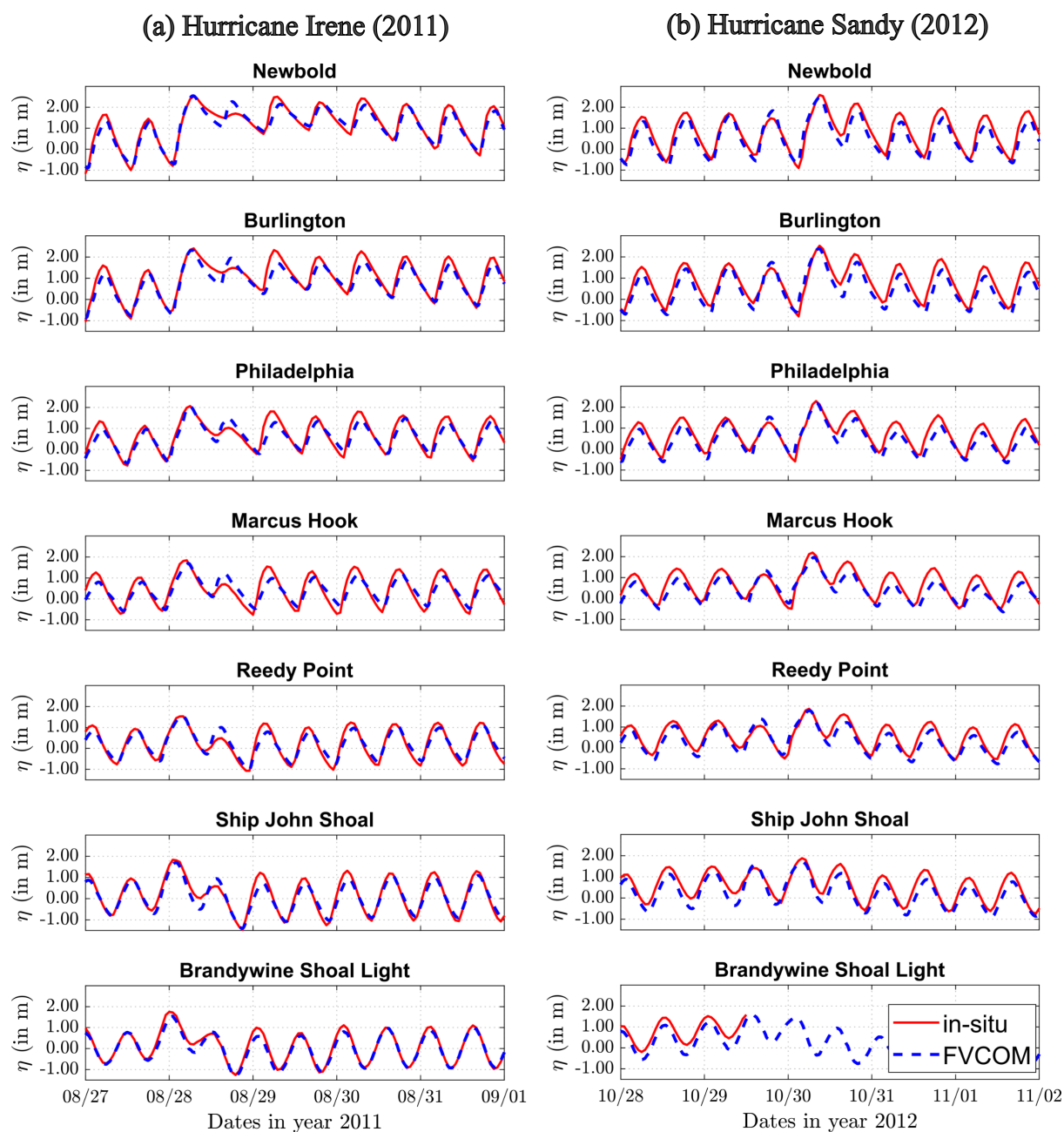
Figure C1. Water surface elevation comparison between model results and in situ (in meters) at NOAA tide gauge locations in Delaware Bay and River during (a) Hurricane Irene (2011) and (b) Hurricane Sandy (2012).
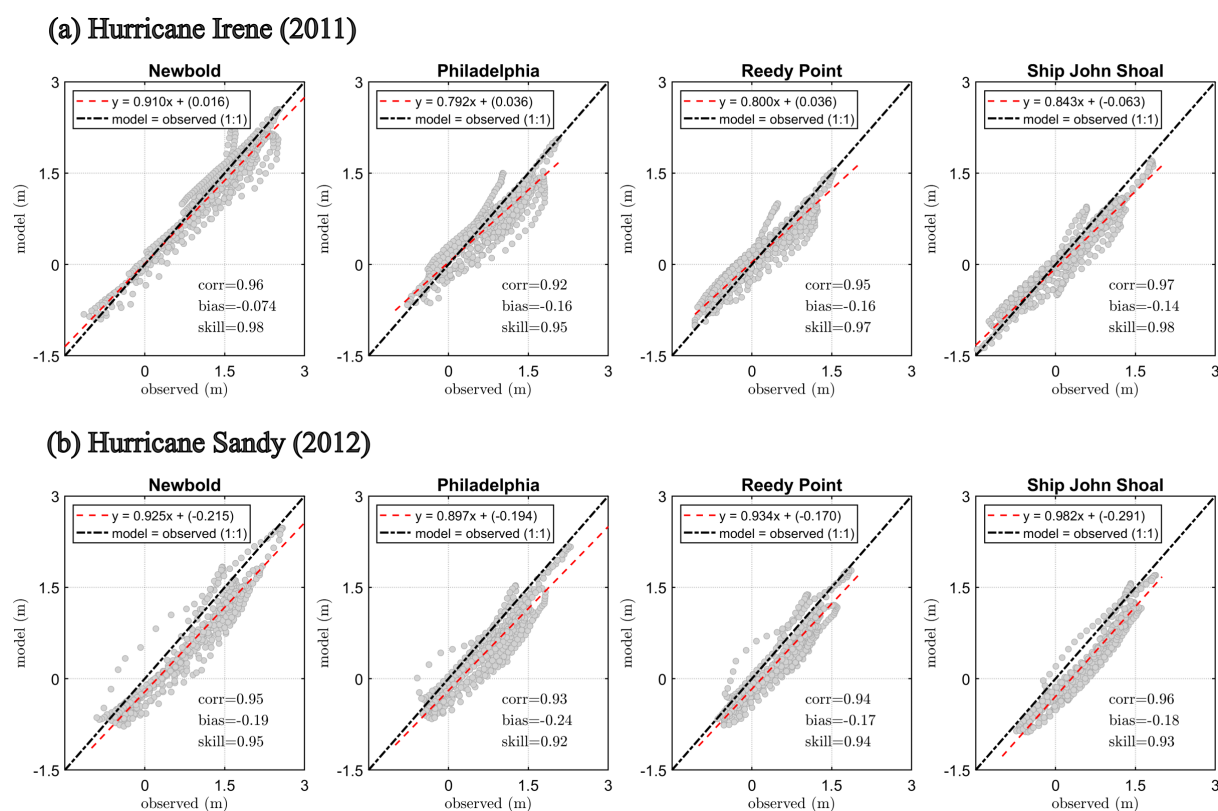
Figure C2. Scatter comparison and statistics for (a) Hurricane Irene (2011) and (b) Hurricane Sandy (2012) water surface elevation at four NOAA tide gauge locations that represent different bay and river zones, going from the upstream river to the estuary.

Author contributions. MD, ZY, and RH contributed to the concept of the study. Model simulations and data processing were conducted by MD, JB, and NS. FVCOM grid generation was worked on by MD and TW. The first version of the manuscript was drafted by MD and JB. DJ supervised the research and funding acquisition. All authors discussed the various model performances and results and revised the manuscript.

345

Competing interests. The authors report no conflicts of interest.

Acknowledgements. This work was supported by the MultiSector Dynamics (MSD), Office of Science, Office of Biological and Environmental Research as part of the multi-program, collaborative Integrated Coastal Modeling (ICoM) project. Also, we performed this study in collaboration with the Cross-Cutting (CC) research area of the ICoM project. All model simulations were performed using resources available through Research Computing at Pacific Northwest National Laboratory and the National Energy Research Scientific Computing Center (NERSC), a U.S. Department of Energy Office of Science User Facility located at Lawrence Berkeley National Laboratory operated under Contract No. DE-AC02-05CH11231 using NERSC award BER-ERCAP m3780 for 2022. CPC Global Unified Gauge-Based Analysis of Daily Precipitation data provided by the NOAA PSL, Boulder, Colorado, USA, from their website at https://psl.noaa.gov.

350

References

355   Balaguru, K., Xu, W., Chang, C.-C., Leung, L. R., Judi, D. R., Hagos, S. M., Wehner, M. F., Kossin, J. P., and Ting, M.: Increased U.S. coastal hurricane risk under climate change, Science Advances, 9, eadf0259, https://doi.org/10.1126/sciadv.adf0259, 2023.

Bates, P. D., Quinn, N., Sampson, C., Smith, A., Wing, O., Sosa, J., Savage, J., Olcese, G., Neal, J., Schumann, G., Giustarini, L., Coxon, G., Porter, J. R., Amodeo, M. F., Chu, Z., Lewis-Gruss, S., Freeman, N. B., Houser, T., Delgado, M., Hamidi, A., Bolliger, I., E. McCusker, K., Emanuel, K., Ferreira, C. M., Khalid, A., Haigh, I. D., Couasnon, A., E. Kopp, R., Hsiang, S., and Krajewski, W. F.: Combined Modeling

360   of US Fluvial, Pluvial, and Coastal Flood Hazard Under Current and Future Climates, Water Resources Research, 57, e2020WR028 673, https://doi.org/https://doi.org/10.1029/2020WR028673, e2020WR028673 2020WR028673, 2021.

Bilskie, M. V., Hagen, S. C., Medeiros, S. C., Cox, A. T., Salisbury, M., and Coggin, D.: Data and numerical analysis of astronomic tides, wind-waves, and hurricane storm surge along the northern Gulf of Mexico, Journal of Geophysical Research: Oceans, 121, 3625–3658, https://doi.org/https://doi.org/10.1002/2015JC011400, 2016.

365   Callahan, J. A. and Leathers, D. J.: Estimation of Return Levels for Extreme Skew Surge Coastal Flooding Events in the Delaware and Chesapeake Bays for 1980–2019, Frontiers in Climate, 3, https://doi.org/10.3389/fclim.2021.684834, 2021.

Cangialosi, J. P., Blake, E., DeMaria, M., Penny, A., Latto, A., Rappaport, E., and Tallapragada, V.: Recent Progress in Tropical Cyclone Intensity Forecasting at the National Hurricane Center, Weather and Forecasting, 35, 1913–1922, https://doi.org/10.1175/WAF-D-20-0059.1, 2020.

370   Chen, C., Liu, H., and Beardsley, R. C.: An Unstructured Grid, Finite-Volume, Three-Dimensional, Primitive Equations Ocean Model: Application to Coastal Ocean and Estuaries, Journal of Atmospheric and Oceanic Technology, 20, 159 – 186, https://doi.org/https://doi.org/10.1175/1520-0426(2003)020<0159:AUGFVT>2.0.CO;2, 2003.

Chen, M., Shi, W., Xie, P., Silva, V. B. S., Kousky, V. E., Higgins, R. W., and Janowiak, J. E.: Assessing objective techniques for gauge-based analyses of global daily precipitation, Journal of Geophysical Research, 113, https://doi.org/10.1029/2007jd009132, 2008.

375   Cyriac, R., Dietrich, J., Fleming, J., Blanton, B., Kaiser, C., Dawson, C., and Luettich, R.: Variability in Coastal Flooding predictions due to forecast errors during Hurricane Arthur, Coastal Engineering, 137, 59–78, https://doi.org/10.1016/j.coastaleng.2018.02.008, 2018.

Deb, M., Sun, N., Yang, Z., Wang, T., Judi, D., Xiao, Z., and Wigmosta, M. S.: Interacting Effects of Watershed and Coastal Processes on the Evolution of Compound Flooding During Hurricane Irene, Earth's Future, 11, e2022EF002 947, https://doi.org/https://doi.org/10.1029/2022EF002947, e2022EF002947 2022EF002947, 2023.

380   Defne, Z., Ganju, N. K., and Moriarty, J. M.: Hydrodynamic and Morphologic Response of a Back-Barrier Estuary to an Extratropical Storm, Journal of Geophysical Research: Oceans, 124, 7700–7717, https://doi.org/https://doi.org/10.1029/2019JC015238, 2019.

Dietrich, J., Bunya, S., Westerink, J., Ebersole, B., Smith, J., Atkinson, J., Jensen, R., Resio, D., Luettich, R., Dawson, C., et al.: A High-Resolution Coupled Riverine Flow, Tide, Wind, Wind Wave, and Storm Surge Model for Southern Louisiana and Mississippi. Part II: Synoptic Description and Analysis of Hurricanes Katrina and Rita, Monthly Weather Review, 138, 378 – 404,

385   https://doi.org/https://doi.org/10.1175/2009MWR2907.1, 2010.

Dietrich, J., Zijlema, M., Westerink, J., Holthuijsen, L., Dawson, C., Luettich, R., Jensen, R., Smith, J., Stelling, G., and Stone, G.: Modeling hurricane waves and storm surge using integrally-coupled, scalable computations, Coastal Engineering, 58, 45–65, https://doi.org/https://doi.org/10.1016/j.coastaleng.2010.08.001, 2011.

Egbert, G. D. and Erofeeva, S. Y.: Efficient Inverse Modeling of Barotropic Ocean Tides, Journal of Atmospheric and Oceanic Technology,

390   19, 183 – 204, https://doi.org/https://doi.org/10.1175/1520-0426(2002)019<0183:EIMOBO>2.0.CO;2, 2002.

Emanuel, K.: Increasing destructiveness of tropical cyclones over the past 30 years, Nature, 436, 686–688, 2005.

Emanuel, K.: Response of Global Tropical Cyclone Activity to Increasing CO2: Results from Downscaling CMIP6 Models, Journal of Climate, 34, 57 – 70, https://doi.org/https://doi.org/10.1175/JCLI-D-20-0367.1, 2021.

Familkhalili, R. and Talke, S. A.: The effect of channel deepening on tides and storm surge: A case study of Wilmington, NC, Geophysical Research Letters, 43, 9138–9147, https://doi.org/10.1002/2016GL069494, 2016.

Garner, A. J., Kopp, R. E., and Horton, B. P.: Evolving Tropical Cyclone Tracks in the North Atlantic in a Warming Climate, Earth's Future, 9, e2021EF002 326, https://doi.org/https://doi.org/10.1029/2021EF002326, e2021EF002326 2021EF002326, 2021.

Glahn, B., Taylor, A., Kurkowski, N., and Shaffer, W.: The role of the SLOSH model in National Weather Service storm surge forecasting, National Weather Digest, 33, 3–14, 2009.

Golaz, J.-C., Roekel, L. P. V., Zheng, X., Roberts, A. F., Wolfe, J. D., Lin, W., Bradley, A. M., Tang, Q., Maltrud, M. E., Forsyth, R. M., Zhang, C., Zhou, T., Zhang, K., Zender, C. S., Wu, M., Wang, H., Turner, A. K., Singh, B., Richter, J. H., Qin, Y., Petersen, M. R., Mametjanov, A., Ma, P.-L., Larson, V. E., Krishna, J., Keen, N. D., Jeffery, N., Hunke, E. C., Hannah, W. M., Guba, O., Griffin, B. M., Feng, Y., Engwirda, D., Vittorio, A. V. D., Dang, C., Conlon, L. M., Chen, C.-C.-J., Brunke, M. A., Bisht, G., Benedict, J. J., Asay-Davis, X. S., Zhang, Y., Zhang, M., Zeng, X., Xie, S., Wolfram, P. J., Vo, T., Veneziani, M., Tesfa, T. K., Sreepathi, S., Salinger, A. G., Eyre, J. E. J. R., Prather, M. J., Mahajan, S., Li, Q., Jones, P. W., Jacob, R. L., Huebler, G. W., Huang, X., Hillman, B. R., Harrop, B. E., Foucar, J. G., Fang, Y., Comeau, D. S., Caldwell, P. M., Bartoletti, T., Balaguru, K., Taylor, M. A., McCoy, R. B., Leung, L. R., and Bader, D. C.: The DOE E3SM Model Version 2: Overview of the Physical Model and Initial Model Evaluation, Journal of Advances in Modeling Earth Systems, 14, https://doi.org/10.1029/2022ms003156, 2022.

Gori, A., Lin, N., Xi, D., and Emanuel, K.: Tropical cyclone climatology change greatly exacerbates US extreme rainfall–surge hazard, Nature Climate Change, 12, 171–178, 2022.

Gupta, H. V., Kling, H., Yilmaz, K. K., and Martinez, G. F.: Decomposition of the mean squared error and NSE performance criteria: Implications for improving hydrological modelling, Journal of Hydrology, 377, 80–91, https://doi.org/https://doi.org/10.1016/j.jhydrol.2009.08.003, 2009.

He, F. and Posselt, D. J.: Impact of Parameterized Physical Processes on Simulated Tropical Cyclone Characteristics in the Community Atmosphere Model, Journal of Climate, 28, 9857 – 9872, https://doi.org/https://doi.org/10.1175/JCLI-D-15-0255.1, 2015.

Hersbach, H., Bell, B., Berrisford, P., Hirahara, S., Horányi, A., Muñoz-Sabater, J., Nicolas, J., Peubey, C., Radu, R., Schepers, D., Simmons, A., Soci, C., Abdalla, S., Abellan, X., Balsamo, G., Bechtold, P., Biavati, G., Bidlot, J., Bonavita, M., Chiara, G., Dahlgren, P., Dee, D., Diamantakis, M., Dragani, R., Flemming, J., Forbes, R., Fuentes, M., Geer, A., Haimberger, L., Healy, S., Hogan, R. J., Hólm, E., Janisková, M., Keeley, S., Laloyaux, P., Lopez, P., Lupu, C., Radnoti, G., Rosnay, P., Rozum, I., Vamborg, F., Villaume, S., and Thépaut, J.-N.: The ERA5 global reanalysis, Quarterly Journal of the Royal Meteorological Society, 146, 1999–2049, https://doi.org/10.1002/qj.3803, 2020.

Houston, S. H., Shaffer, W. A., Powell, M. D., and Chen, J.: Comparisons of HRD and SLOSH surface wind fields in hurricanes: Implications for storm surge modeling, Weather and Forecasting, 14, 671–686, 1999.

Hu, K., Ding, P., Wang, Z., and Yang, S.: A 2D/3D hydrodynamic and sediment transport model for the Yangtze Estuary, China, Journal of Marine Systems, 77, 114–136, https://doi.org/https://doi.org/10.1016/j.jmarsys.2008.11.014, 2009.

Huang, B., Liu, C., Banzon, V., Freeman, E., Graham, G., Hankins, B., Smith, T., and Zhang, H.-M.: Improvements of the Daily Optimum Interpolation Sea Surface Temperature (DOISST) Version 2.1, Journal of Climate, 34, 2923 – 2939, https://doi.org/https://doi.org/10.1175/JCLI-D-20-0166.1, 2021.

Jelesnianski, C. P.: SLOSH: Sea, lake, and overland surges from hurricanes, vol. 48, US Department of Commerce, National Oceanic and
430   Atmospheric Administration . . . , 1992.

Knapp, K. R., Kruk, M. C., Levinson, D. H., Diamond, H. J., and Neumann, C. J.: The International Best Track Archive for Climate
Stewardship (IBTrACS), Bulletin of the American Meteorological Society, 91, 363–376, https://doi.org/10.1175/2009bams2755.1, 2010.

Knapp, K. R., Diamond, H. J., Kossin, J. P., Kruk, M. C., and Schreck, C. J.: International Best Track Archive for Climate Stewardship
(IBTrACS) Project, Version 4, https://doi.org/10.1175/2009bams2755.1, accessed October 2022., 2018.

435   Knutson, T. R., Sirutis, J. J., Bender, M. A., Tuleya, R. E., and Schenkel, B. A.: Dynamical downscaling projections of late twenty-first-
century U.S. landfalling hurricane activity, Climatic Change, 171, 28, https://doi.org/10.1007/s10584-022-03346-7, 2022.

Lin, N., Emanuel, K. A., Smith, J. A., and Vanmarcke, E.: Risk assessment of hurricane storm surge for New York City, Journal of Geophys-
ical Research: Atmospheres, 115, https://doi.org/https://doi.org/10.1029/2009JD013630, 2010.

Lin, N., Marsooli, R., and Colle, B. A.: Storm surge return levels induced by mid-to-late-twenty-first-century extratropical cyclones in the
440   Northeastern United States, Climatic change, 154, 143–158, 2019.

Lyddon, C., Brown, J. M., Leonardi, N., and Plater, A. J.: Uncertainty in estuarine extreme water level predictions due to surge-tide interac-
tion, PLOS ONE, 13, e0206 200, https://doi.org/10.1371/journal.pone.0206200, 2018.

Marsooli, R. and Lin, N.: Numerical Modeling of Historical Storm Tides and Waves and Their Interactions Along the U.S. East and Gulf
Coasts, Journal of Geophysical Research: Oceans, 123, 3844–3874, https://doi.org/https://doi.org/10.1029/2017JC013434, 2018.

445   Marsooli, R., Lin, N., Emanuel, K., and Feng, K.: Climate change exacerbates hurricane flood hazards along US Atlantic and Gulf Coasts in
spatially varying patterns, Nature communications, 10, 3785, 2019.

Mori, N., Kato, M., Kim, S., Mase, H., Shibutani, Y., Takemi, T., Tsuboki, K., and Yasuda, T.: Local amplification of storm surge by Super
Typhoon Haiyan in Leyte Gulf, Geophysical Research Letters, 41, 5106–5113, https://doi.org/10.1002/2014GL060689, 2014.

Perkins, W. A., Duan, Z., Sun, N., Wigmosta, M. S., Richmond, M. C., Chen, X., and Leung, L. R.: Parallel Dis-
450   tributed Hydrology Soil Vegetation Model (DHSVM) using global arrays, Environmental Modelling Software, 122, 104 533,
https://doi.org/https://doi.org/10.1016/j.envsoft.2019.104533, 2019.

Powell, M. D. and Houston, S. H.: Hurricane Andrew's landfall in south Florida. Part II: Surface wind fields and potential real-time applica-
tions, Weather and Forecasting, 11, 329–349, 1996.

Rego, J. L. and Li, C.: On the importance of the forward speed of hurricanes in storm surge forecasting: A numerical study: FORWARD
455   SPEED OF A HURRICANE, Geophysical Research Letters, 36, n/a–n/a, https://doi.org/10.1029/2008GL036953, 2009.

Resio, D. T. and Westerink, J. J.: Modeling the physics of storm surges, Physics Today, 61, 33–38, https://doi.org/10.1063/1.2982120, 2008.

Roberts, M. J., Camp, J., Seddon, J., Vidale, P. L., Hodges, K., Vannière, B., Mecking, J., Haarsma, R., Bellucci, A., Scoccimarro, E.,
Caron, L.-P., Chauvin, F., Terray, L., Valcke, S., Moine, M.-P., Putrasahan, D., Roberts, C. D., Senan, R., Zarzycki, C., Ullrich, P.,
Yamada, Y., Mizuta, R., Kodama, C., Fu, D., Zhang, Q., Danabasoglu, G., Rosenbloom, N., Wang, H., and Wu, L.: Projected Future
460   Changes in Tropical Cyclones Using the CMIP6 HighResMIP Multimodel Ensemble, Geophysical Research Letters, 47, e2020GL088 662,
https://doi.org/https://doi.org/10.1029/2020GL088662, e2020GL088662 2020GL088662, 2020.

Shen, J., Gong, W., and Wang, H. V.: Water level response to 1999 Hurricane Floyd in the Chesapeake Bay, Continental Shelf Research, 26,
2484–2502, https://doi.org/10.1016/j.csr.2006.07.021, 2006a.

Shen, J., Wang, H., Sisson, M., and Gong, W.: Storm tide simulation in the Chesapeake Bay using an unstructured grid model, Estuarine,
465   Coastal and Shelf Science, 68, 1–16, https://doi.org/10.1016/j.ecss.2005.12.018, 2006b.

Sun, N., Yearsley, J., Voisin, N., and Lettenmaier, D. P.: A spatially distributed model for the assessment of land use impacts on stream temperature in small urban watersheds, Hydrological Processes, 29, 2331–2345, https://doi.org/https://doi.org/10.1002/hyp.10363, 2015.

Taylor, A. A. and Glahn, B.: Probabilistic guidance for hurricane storm surge, in: 19th Conference on probability and statistics, vol. 74, 2008.

Valle-Levinson, A., Olabarrieta, M., and Heilman, L.: Compound flooding in Houston-Galveston Bay during Hurricane Harvey, Science of The Total Environment, 747, 141 272, https://doi.org/https://doi.org/10.1016/j.scitotenv.2020.141272, 2020.

Villarini, G., Goska, R., Smith, J. A., and Vecchi, G. A.: North Atlantic Tropical Cyclones and U.S. Flooding, Bulletin of the American Meteorological Society, 95, 1381 – 1388, https://doi.org/https://doi.org/10.1175/BAMS-D-13-00060.1, 2014.

Wahl, T., Jain, S., Bender, J., Meyers, S. D., and Luther, M. E.: Increasing risk of compound flooding from storm surge and rainfall for major US cities, Nature Climate Change, 5, 1093–1097, 2015.

Wang, S., McGrath, R., Hanafin, J., Lynch, P., Semmler, T., and Nolan, P.: The impact of climate change on storm surges over Irish waters, Ocean Modelling, 25, 83–94, https://doi.org/https://doi.org/10.1016/j.ocemod.2008.06.009, 2008.

Weaver, M. M. and Garner, A. J.: Varying genesis and landfall locations for North Atlantic tropical cyclones in a warmer climate, Scientific Reports, 13, 5482, https://doi.org/10.1038/s41598-023-31545-4, 2023.

Weisberg, R. H. and Zheng, L.: Hurricane storm surge simulations for Tampa Bay, Estuaries and Coasts, 29, 899–913, https://doi.org/10.1007/BF02798649, 2006.

Weisberg, R. H. and Zheng, L.: Hurricane storm surge simulations comparing three-dimensional with two-dimensional formulations based on an Ivan-like storm over the Tampa Bay, Florida region, Journal of Geophysical Research: Oceans, 113, https://doi.org/https://doi.org/10.1029/2008JC005115, 2008.

Wigmosta, M. S., Vail, L. W., and Lettenmaier, D. P.: A distributed hydrology-vegetation model for complex terrain, Water resources research, 30, 1665–1679, 1994.

Wong, K.-C. and Moses-Hall, J. E.: On the relative importance of the remote and local wind effects to the subtidal variability in a coastal plain estuary, Journal of Geophysical Research: Oceans, 103, 18 393–18 404, https://doi.org/https://doi.org/10.1029/98JC01476, 1998.

Wong, K.-C. and Trowbridge, J. H.: Some observational evidence on the effect of atmospheric forcing on tidal variability in the upper Delaware Bay, Journal of Geophysical Research, 95, 16 229, https://doi.org/10.1029/JC095iC09p16229, 1990.

Xiao, Z., Yang, Z., Wang, T., Sun, N., Wigmosta, M., and Judi, D.: Characterizing the Non-linear Interactions Between Tide, Storm Surge, and River Flow in the Delaware Bay Estuary, United States, Frontiers in Marine Science, 8, https://doi.org/10.3389/fmars.2021.715557, 2021.